BIOPHYSICS

Programming PAM antennae for efficient CRISPR-Cas9 DNA editing

Fei Wang[1,2], Yaya Hao[2], Qian Li[2], Jiang Li[3,4], Honglu Zhang[5], Xueli Zhang[1], Lihua Wang[3,6], Carlos Bustamante[5]*, Chunhai Fan[2]*

Bacterial CRISPR-Cas9 nucleases have been repurposed as powerful genome editing tools. Whereas engineering guide RNAs or Cas nucleases have proven to improve the efficiency of CRISPR editing, modulation of protospacer-adjacent motif (PAM), indispensable for CRISPR, has been less explored. Here, we develop a DNA origami–based platform to program a PAM antenna microenvironment and address its performance at the single-molecule level with submolecular resolution. To mimic spatially controlled in vivo PAM distribution as may occur in chromatin, we investigate the effect of PAM antennae surrounding target DNA. We find that PAM antennae effectively sensitize the DNA cleavage by recruiting Cas9 molecules. Super-resolution tracking of single single-guide RNA/Cas9s reveals localized translocation of Cas9 among spatially proximal PAMs. We find that the introduction of the PAM antennae effectively modulates the microenvironment for enhanced target cleavage (up to ~50%). These results provide insight into factors that promote more efficient genome editing.

INTRODUCTION

CRISPR-Cas9 has become a versatile tool for genome editing, diagnosis, and therapeutics (*1*–*3*). With a single-guide RNA (sgRNA), Cas9 can recognize a specific 20–base pair (bp) sequence flanked by a 3-base protospacer-adjacent motif (PAM) (*4*). Genome editing with CRISPR-Cas9 has been performed on bacteria (*5*), plants (*6*), animals (*7*), and even humans (*8*), holding great promise of future treatment of human diseases. Despite the enormous progress achieved so far, a critical technical hurdle is the target site editing efficiency, especially on large genomes (*9*, *10*). To this end, many efforts have been focused on sequence optimization, chemical modifications of sgRNA, or reengineering of Cas nucleases (*11*–*16*). For example, introducing chemical modifications on sgRNA increased gene-editing activity via the reduction of susceptibility of this component to nuclease degradation (*15*). Algorithms have also been developed to consider target sequence features such as its position within the gene or chromatin (*11*). A number of reengineered versions of Cas nucleases have also been reported to have better targeting ability and cleavage efficiency (*14*, *17*).

Recruitment of sgRNA/Cas9 to target sites by PAM and its activation of the nuclease domain of Cas9 are indispensable for CRISPR editing (*18*–*21*). Variation of the PAM density has been shown to affect target binding by Cas9, but modulation of the PAM microenvironment has been less explored for gene editing. Studies of the effect of PAM's spatial distribution and density may lead to alternative strategies to engineer CRISPR editing and contribute to better understanding of gene editing in complex environments (e.g., in chromatin).

DNA origami technology provides a powerful means to organize nanoscale objects with molecular and submolecular precision and addressability (*22*, *23*). Using this approach, individual molecules of nucleic acids and proteins can be site-specifically deposited on a "canvas" over distances ranging from tens to hundreds of nanometers, and their reactions can be easily monitored with optical or atomic force microscopy (AFM) (*24*–*26*). Origami-based platforms are thus particularly useful for studying biomolecular interactions at the single-molecule level (*27*, *28*). In this work, we design DNA origami–confined PAM antennae in the vicinity of a target, providing a microenvironment to investigate the impact of the spatial distribution of PAM on target cleavage efficiency. We study the dynamic process of sgRNA/Cas9 binding in the presence/absence of PAM antennae and program the PAM antennae for more efficient DNA editing.

RESULTS

PAM antenna on DNA origami

To create a local PAM environment for CRISPR-Cas9–based binding and target cleavage in vitro, we used a two-dimensional, rectangular-shaped DNA origami as a template to site-specifically arrange the sgRNA/Cas9 components (Fig. 1A and figs. S1 and S2). The double-stranded DNA (dsDNA) target was placed at the center of the origami (Fig. 1B, black area). To arrange the PAM antenna, we extended eight staple strands adjacent to the target site from the 3′ end, followed by hybridization with a short single-stranded DNA (ssDNA) containing six PAM sites (Fig. 1B), forming a PAM-rich region of ~12 nm by 11 nm (referred to as origami P). Four biotin molecules were modified on the backside of the DNA origami to immobilize it on the avidin-coated surface of glass slides. Controls were prepared by assembling blank origami (referred to as origami B) with the target alone. AFM topography images revealed the presence of a PAM island at the center of origami P, with a full width at half maximum of ~16 nm (Fig. 1, C and D, and fig. S3), consistent with

[1]Joint Research Center for Precision Medicine, Shanghai Jiao Tong University Affiliated Sixth People's Hospital South Campus, Southern Medical University Affiliated Fengxian Hospital, Shanghai 201499, China. [2]School of Chemistry and Chemical Engineering, Frontiers Science Center of Transformative Molecules, and Institute of Molecular Medicine, Renji Hospital, School of Medicine, Shanghai Jiao Tong University, Shanghai 200240, China. [3]CAS Key Laboratory of Interfacial Physics and Technology, Shanghai Institute of Applied Physics, Chinese Academy of Sciences, Shanghai 201800, China. [4]Shanghai Synchrotron Radiation Facility, Zhangjiang Laboratory, Shanghai Advanced Research Institute, Chinese Academy of Sciences, Shanghai 201210, China. [5]Department of Chemistry, Institute for Quantitative Biosciences (QB3), Department of Physics, Department of Molecular and Cell Biology, Kavli Energy Nanosciences Institute at Berkeley, Howard Hughes Medical Institute, University of California, Berkeley, Berkeley, CA 94720, USA. [6]Shanghai Key Laboratory of Green Chemistry and Chemical Processes, School of Chemistry and Molecular Engineering, East China Normal University, 500 Dongchuan Road, Shanghai, 200241, China. *Corresponding author. Email: carlosb@berkeley.edu (C.B.); fanchunhai@sjtu.edu.cn (C.F.)

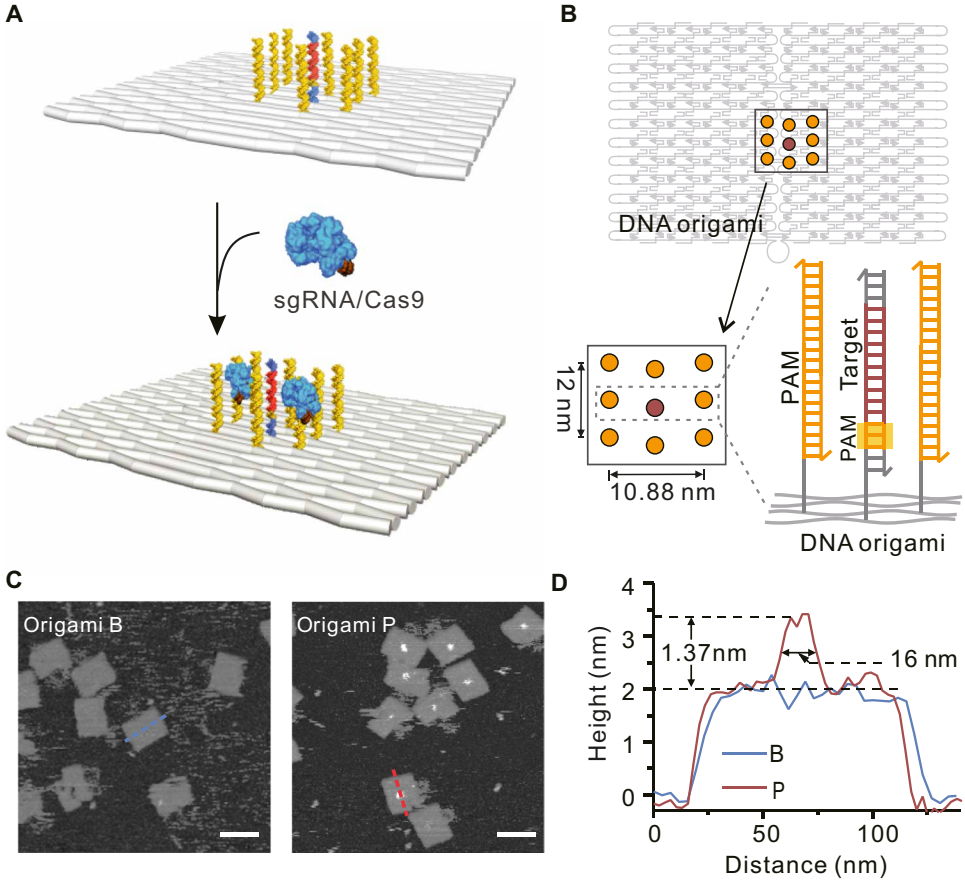

Fig. 1. Structural design of PAM antenna on DNA origami. (**A**) Schematic illustration of a local PAM environment that could recruit sgRNA/Cas9 molecule on a rectangular DNA origami. (**B**) Schematics for design and construction of origami P with a PAM antenna (yellow dots) surrounding the target (red dots). Target dsDNA has a 20-bp target sequence for hybridization with sgRNA (red) and a 3-bp PAM sequence (highlighted in yellow). Each antenna duplex containing six PAM sites (5′-NGG-3′) protrudes from a staple strand, which can bind to sgRNA/Cas9 transiently. (**C**) AFM images of origami B (left) and origami P (right). Scale bars, 100 nm. (**D**) Profile along dashed lines in (C) showing a higher region on origami P.

the expected width of DNA strands and confirming the formation of a nanoscale local environment of PAM.

We next explored how the PAM antenna affected Cas9 binding. We monitored the binding events of Cy5-labeled sgRNA/Cas9 with the target DNA localized on origami B and P, respectively. To this end, we hybridized a 3′-end extended sgRNA with a Cy5-tagged short ssDNA strand (fig. S4). To avoid cleavage, we used catalytically inactive Cas9 (dCas9) in these experiments. Binding dynamics of dCas9 was characterized by analyzing the variation of the fluorescence intensity at the target DNA position with time. We found that the occurrence of binding events on origami P (94 ± 1.8%) was considerably higher than that on origami B (68 ± 3.5%) (Fig. 2A and fig. S5). The distribution of binding events on individual origami revealed a considerable enrichment of dCas9 on origami P over that observed on origami B with a considerably higher multiple binding ($n > 1$) probability, suggesting that PAM antennae operate as dCas9-binding hotspots.

Next, we investigated the binding efficiency of dCas9 on origami with antennae using AFM. Besides origami P and B, origami harboring non-PAM antennae (referred to as origami N) were assembled with the same local spatial environment as origami P. AFM height profiling was used to study the static binding of sgRNA/dCas9 on origami B, N, and P. Binding to the origami was manifested as a height increase in their center region (Fig. 2B and fig. S6). Height profile analysis revealed that sgRNA/dCas9 bound to all origami with the target DNA; however, the presence of the PAM antennae led to an increase of ~31% in the binding efficiency, which coincides well with the observations in the kinetic studies described above.

To substantiate the idea that PAM antennae represent binding hotspots for Cas9, we perform Markov chain simulations to investigate the movement of the nuclease on antenna-carrying origami (Fig. 2C). Transient interactions between Cas9 and PAM antenna were modeled by scaling binding and dissociating rates (blank model with no binding, non-PAM antenna model with high binding rate and high dissociation rate, and PAM antenna model with high binding rate and low dissociation rate). Counting the number of occurrences of Cas9 in each spatial unit, we obtained a heatmap exhibiting the probability distribution for Cas9 to appear at each unit. The heatmap showed ~2-fold higher intensity near the PAM antenna for a 5:1 ratio of binding and dissociation rates, representing a Cas9-binding hotspot due to the strong enhancement by the surrounding PAM antenna.

PAM antennae enhance target cleavage

Having established that PAM antennae enhance Cas9 binding, we next explored the effect of PAM microenvironments on target cleavage at the single-molecule level. AFM imaging of origami B

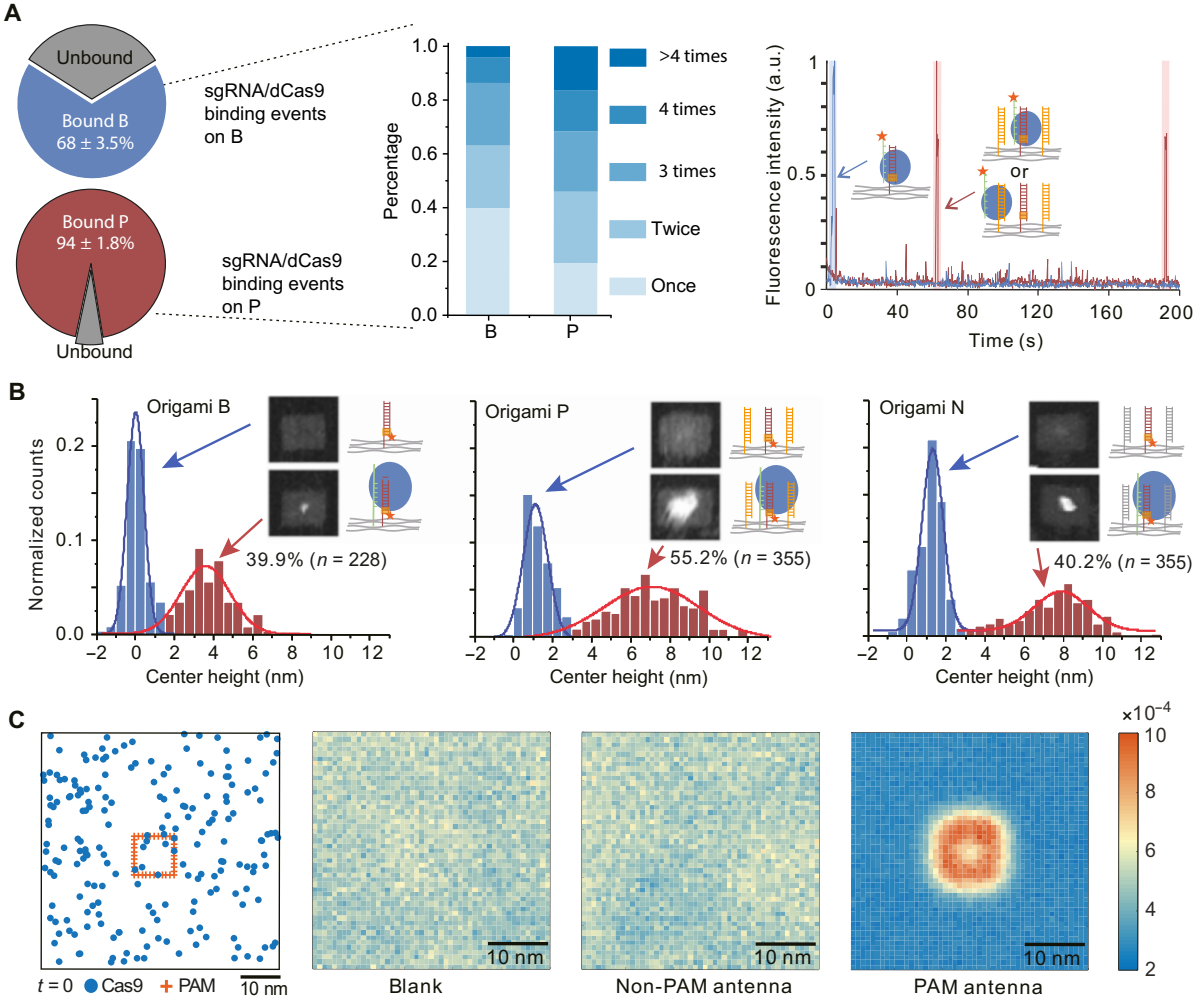

Fig. 2. PAM antenna creates Cas9-binding hotspot on a rectangular DNA origami. (**A**) Left: The frequency of binding events on origami P is higher than that on origami B. Middle: Statistics of the number of binding events on each origami during the observation period shows the enrichment of sgRNA/dCas9 on origami P. Right: Sample intensity–time traces at an individual target position of origami B (blue) and P (red) showing single dCas9 binding event on origami B and two dCas9 binding events on origami P. a.u., arbitrary units. (**B**) Center height distribution showing two peaks corresponding to AFM topographic images of bound and unbound DNA origami. State composition (red bars for the bound state and blue bars for the unbound state) shows a higher bound percentage on origami P ($n = 355$, $P = 55.2\%$) over origami B ($n = 228$, $P = 39.9\%$) and origami N ($n = 355$, $P = 40.2\%$). (**C**) Heatmaps showing that the spatial distribution of Cas9 is rearranged with PAM antennae, whereas non-PAM antennae with high dissociation rate had no obvious effect on Cas9 distribution. For the initial condition, Cas9 molecules were randomly placed in a 60 nm–by–60 nm region.

before and after incubating with sgRNA/Cas9 showed that most origami (>85%) were occupied by sgRNA/Cas9 (fig. S7), suggesting that Cas9 remained tightly bound to both cleaved ends of the target strand (TS; Fig. 3A and fig. S8) and therefore could not be used to monitor the cleavage event. To monitor cleavage, we used instead total internal reflection fluorescence microscopy (TIRFM) to observe the fluorescence variation of Cy3-labeled of either the PAM-proximal or PAM-distal ends on the non-TS (NTS; Fig. 3B). A large fraction of Cy3 fluorescence rapidly disappeared when Cy3 was labeled on the PAM-proximal end (Fig. 3B), indicating cleavage and release of the Cy3-labeled fragments. Control experiments were conducted by injecting buffer without sgRNA/Cas9, which confirmed that the fluorescence disappearance was caused by target cleavage and release (fig. S9). By contrast, when Cy3 was labeled on the PAM-distal end (Fig. 3C), the release process was notably slower. In the following studies, the PAM-proximal end of the NTS was labeled for accurate characterization of target cleavage.

Next, we quantitatively studied the kinetics of the cleavage process by analyzing the time-dependent intensity traces derived from real-time TIRFM imaging. The lifetime of individual target DNA molecules was determined by the time point at which the fluorescence intensity dropped to baseline (Fig. 3B). We next monitored the target cleavage on origami B, N, and P, respectively, to explore the effect of PAM antennae. The individual lifetimes yielded the accumulated cleavage fraction over time. We performed three repeated experiments to obtain averaged cleavage fraction with error bars (Fig. 3D). We found that the cleaved fraction for targets on origami P harboring PAM antennae was significantly higher (87 ± 4%) than that on origami B (77 ± 1%) and N (74 ± 3%), suggesting that the presence of PAM antennae significantly enhanced target cleavage efficiency.

Several studies showed that CRISPR-Cas9 can edit genome loci in different spatial contexts (*29*). To investigate whether CRISPR cleavage is affected by the structure of the local environment, we compared the cleavage of targets surrounded by non-PAM–containing

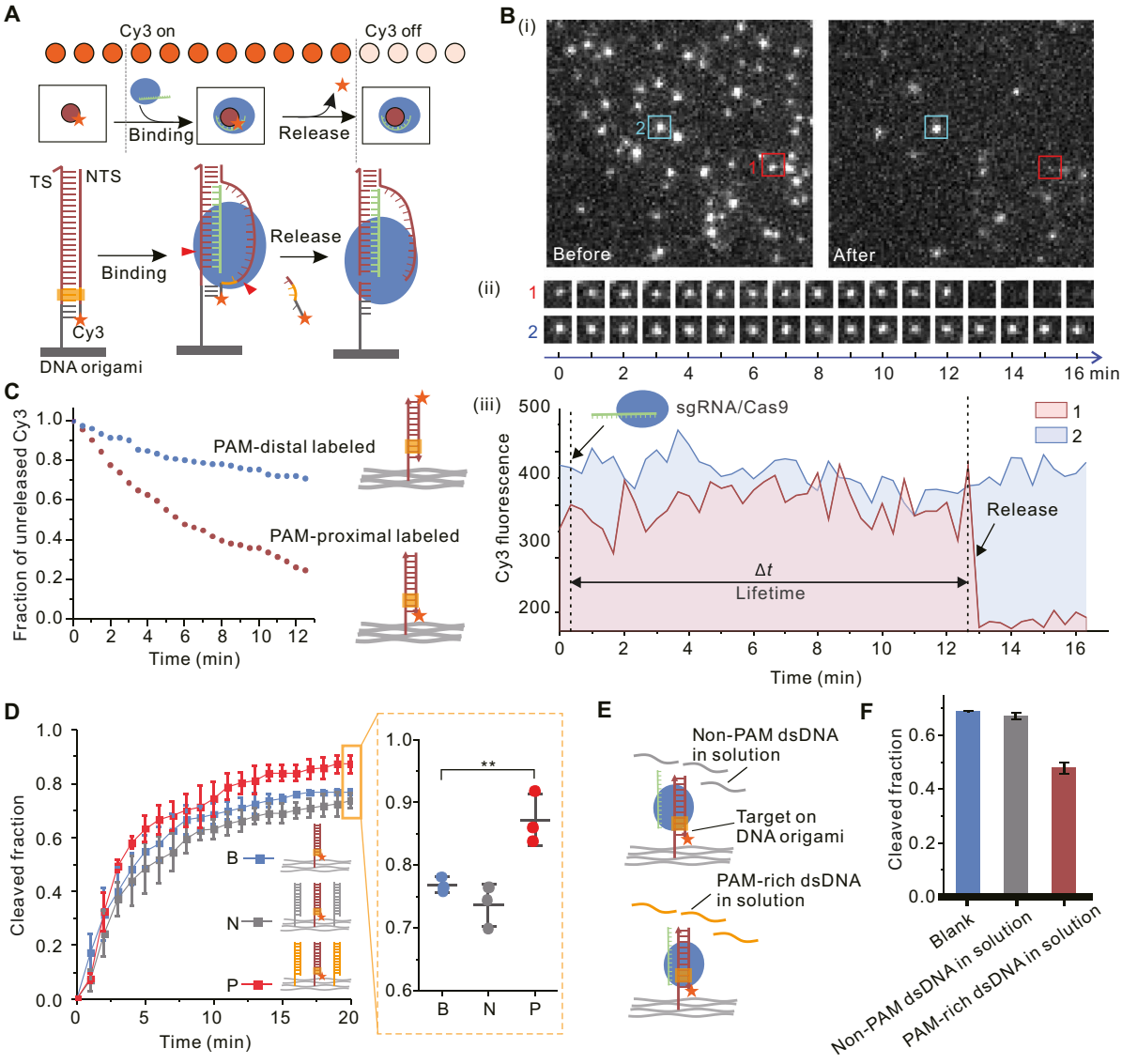

Fig. 3. Enhanced target cleavage induced by PAM antenna. (**A**) Schematic illustration of the state of the Cy3 label corresponding to the binding of sgRNA/Cas9 and the release of cleaved fragment. NTS, non-TS. (**B**) Target cleavage and release kinetics imaged using TIRFM. (i) A representative imaging field under TIRFM before (left) and 15 min after injection of sgRNA/Cas9 (right) when Cy3 is labeled on the PAM-proximal end of NTS. (ii) Snapshots of two targets in the imaging field at the indicated time points. (iii) Cleavage kinetics showing the lifetime of sgRNA/Cas9 for the two targets in (ii). (**C**) Fraction of unreleased Cy3 decays with time for Cy3 labeled on the PAM-proximal end (red) and PAM-distal end (blue) of NTS. (**D**) Curve of cleaved fraction calculated from single-molecule assay of origami N, P, and B. The zoomed-in view shows cleaved fraction within 20 min after injecting sgRNA/Cas9 to origami N, P, and B. Data are mean ± SD ($n = 3$ independent experiments). $^{**}P = 0.01$ (unpaired, two-sided t test). (**E**) Schematics depicting the binding of sgRNA/Cas9 to target on origami B with non-PAM dsDNA and PAM-rich dsDNA in solution. (**F**) Cleaved fraction within 20 min after injecting sgRNA/Cas9 to origami B with blank, non-PAM dsDNA, and PAM-rich dsDNA in solution. Error bars represent SD for three independent experiments.

antennae (origami N) with that of targets in antenna-free origami (origami B). Cleavage fraction measurements showed no significant difference between origami N and B (Fig. 3D), suggesting that Cas9 binding and cleavage were not significantly affected by the spatial organization of non-PAM sequences. This independence was also shown in dCas9-binding measurements (Fig. 2B).

To determine whether the formation of a structured PAM environment is required for enhanced target cleavage, we tested whether freely diffusive antenna strands affect target cleavage (Fig. 3E). The presence of 1 μM non-PAM strands in the reaction buffer showed no obvious influence on target cleavage (Fig. 3F), which is consistent with the effect of non-PAM antennae. However, the presence of 1 μM PAM strands in the reaction buffer remarkably decreased the cleaved fraction of target by 30%, which is consistent with previous studies that show that PAM-containing dsDNA added in trans act as competitors to the specific target (*18*, *30*). Compared to the enhancing effect of PAM antennae on DNA origami, the inhibiting effect of freely diffusive PAM antenna strands in the reaction buffer indicates that the confinement of PAM antennae into a structured environment was necessary for cleavage efficiency enhancement.

Localized diffusion of Cas9 within PAM antennae

To investigate the mechanism by which PAM antennae improve the target cleavage efficiency, we tracked the movement of dCas9 within

the PAM antennae at the single-molecule level. Specifically, we localized the position of fluorescently labeled sgRNA/dCas9 after their binding to the origami. Analysis of time trajectories of individual dCas9 reveals a remarkably larger range of displacement on origami P than on origami B (Fig. 4B and fig. S10). Statistical analysis of dCas9 displacement from its initial position revealed that the maximum displacement range of dCas9 in 200-ms time interval on origami B was within 40 nm, reflecting the range of displacement of tightly bound dCas9 (Fig. 4A). In contrast, on origami P, this range of displacement increases to nearly ~80 nm, suggesting the localized diffusion of dCas9 among the PAM antennae (Fig. 4B). An origami on which PAM-rich antennae were placed remotely from the target (origami O; fig. S11A) was used to study the dependence of localized diffusion on target-PAM antenna distance. Both binding and cleavage results showed that remotely located PAM-rich regions do not favor the transfer of Cas9 to the target as efficiently as when they are placed in the proximal environment of the target (figs. S11 and S12).

To further study how the localized diffusion mechanism of Cas9 within the PAM microenvironments results in enhanced target cleavage, we numerically simulated the spatial distribution of unbound Cas9 using a random walk model (Fig. 4C). In this model, Cas9 performs localized diffusion with a short step length inside PAM antenna and free diffusion with a long step length outside. To qualitatively study the effect of localized diffusion on the spatial distribution of Cas9, we simplified the PAM microenvironment into a 10.5 nm–by–10.5 nm area with uniformly distributed 49 PAMs, and the target site was set at the center of this area. Initially, Cas9s were uniformly distributed in a 60 nm–by–60 nm region (fig. S13A). By counting the number of occurrences of unbound Cas9 in each spatial unit, we obtained a heatmap exhibiting the probability distribution for unbound Cas9 to appear at each location. The heatmap showed an increased probability of finding Cas9 inside PAM antennae and reached a maximum near the center (Fig. 4D). The increased probability for the unbound Cas9 to appear at the target site concurs with our experimental results of binding and cleavage assay on origami P, indicating that localized targeting diffusion has a positive effect on target binding. In contrast, a model of the freely diffusing Cas9 inside and outside PAM antennae predicted a uniform spatial distribution of unbound Cas9 that showed no increased distribution at the center, suggesting that localized diffusion mode is essential for target binding enhancement. These observations, combined with the single-molecule tracking results, indicate that the PAM-rich origami microenvironment enhances target cleavage through a localized search diffusional mechanism, which is distinctly different from that operating in solution.

Programming of PAM antennae to modulate the target microenvironment

Because the facilitated targeting of Cas9 by the antennae is distance dependent (fig. S11), we investigated whether the effects of the PAM microenvironment could be modulated through the programming of PAM antennae. We first synthesized two-layered PAM antennae on DNA origami (Fig. 5A, middle). AFM images showed a PAM island larger than that observed with regular antennae (Fig. 5B). We then assessed the effect of the outer-layered PAM antennae on target cleavage. Real-time cleavage assays showed no significant difference on either two-layered antenna origami or origami P (Fig. 5C), indicating that the outer-layered PAM antenna did not contribute to enhanced target cleavage. This result is consistent with our observation that remote PAM does not contribute to Cas9's binding

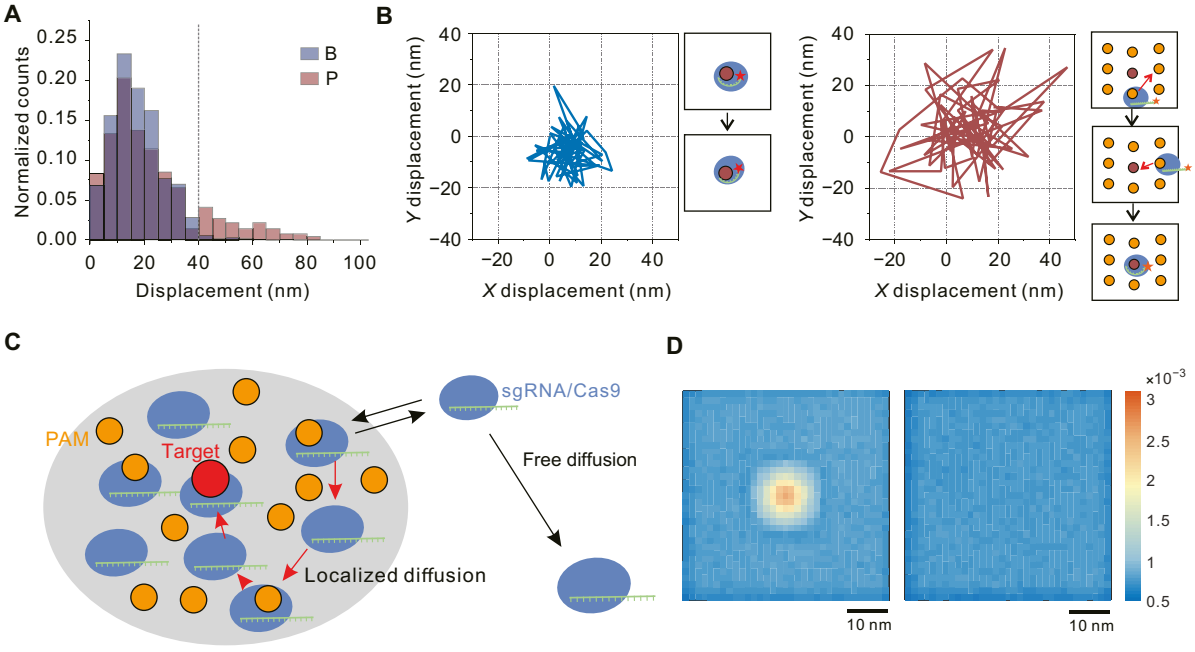

Fig. 4. Localized diffusion mode target search increases target binding. (**A**) Displacement distribution of dCas9 obtained from trajectories on origami B and P. (**B**) Difference in trajectories of sgRNA/dCas9 on origami B (left) and P (right) suggests diffusion of sgRNA/dCas9 among PAMs. (**C**) Possible modes for target searching of sgRNA/Cas9 within PAM antenna including localized diffusion inside PAM antennae and free diffusion in solution. (**D**) Left: Localized diffusion inside PAM microenvironment increases the probability of finding unbound Cas9 at the target location (center position). Right: The probability distribution of unbound Cas9 shows no change when the nuclease is allowed to display only free diffusion inside PAM antennae.

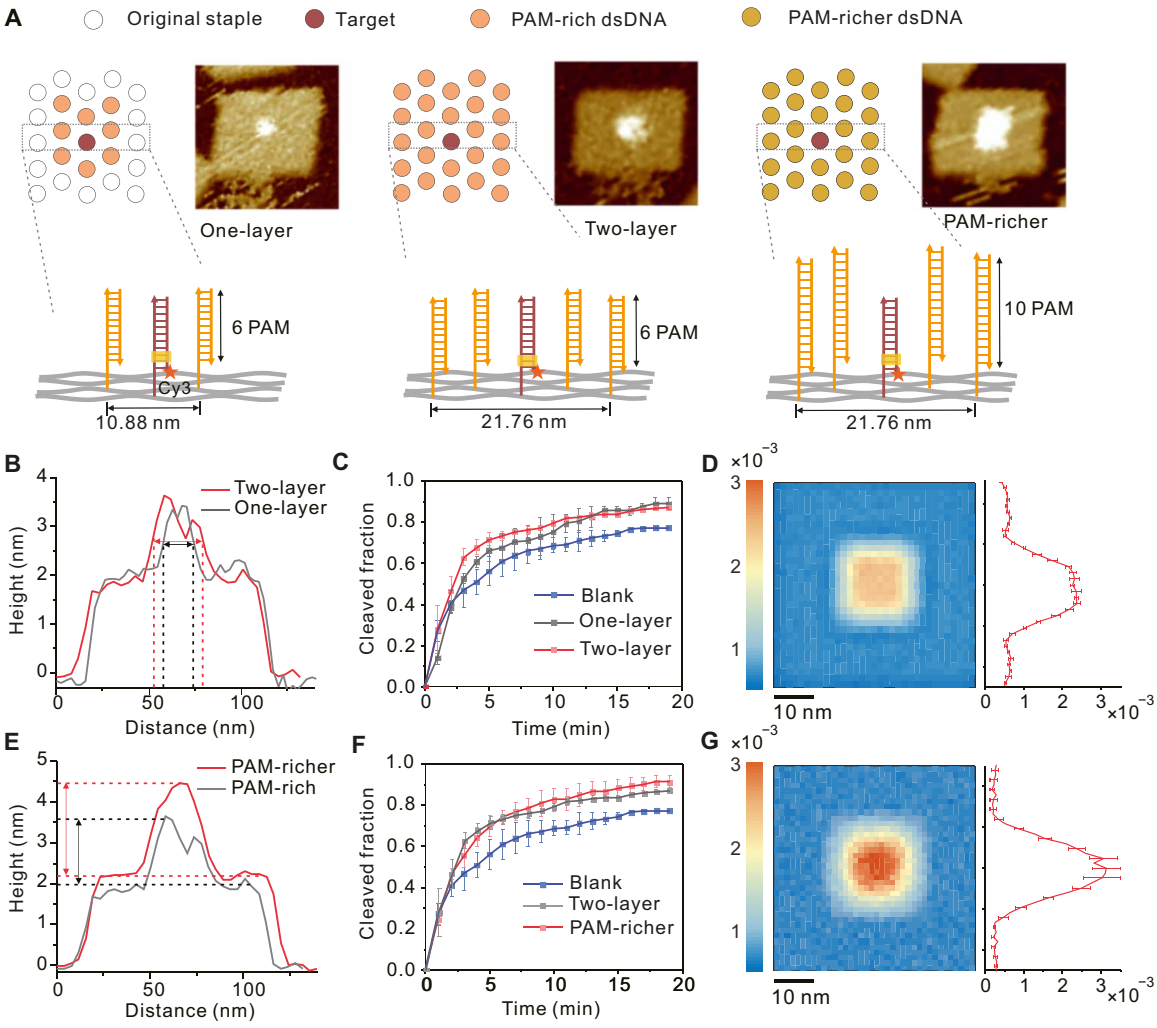

Fig. 5. Programming PAM antenna for microenvironment modulation. (**A**) Schematic design and AFM characterization of one-layered PAM antenna (left; origami P), two-layered PAM antenna (middle), and PAM-richer antenna (right) on DNA origami. (**B**) Profiles of one- and two-layered PAM antenna on DNA origami. (**C**) Curve of cleaved fraction showing that the outer layer of PAM antenna does not contribute to cleavage enhancement. Error bars represent SD for three independent experiments. (**D**) A larger spatial range of PAM antennae does not increase the appearance probability of unbound Cas9 inside the PAM antennae region. Error bars represent SD for five independent simulations. (**E**) Profiles of two-layered PAM and PAM-richer antenna on DNA origami. (**F**) Curve of cleaved fraction showing that PAM-richer antenna induces higher target cleavage efficiency. Error bars represent SD for three independent experiments. (**G**) Numerical simulations suggest that higher PAM density leads to an increase in appearance probability of unbound Cas9 inside the antennae. Error bars represent SD for five independent simulations.

to target. To better understand this result, we simulated the spatial distribution of unbound Cas9 appearance probability in the presence of a larger PAM area (18 nm by 18 nm) using the localized diffusion model. We found that the appearance probability at the center was identical to that of the 10.5-nm PAM antenna model (Fig. 5D). It is possible that the increased capture, associated with the use of more PAMs, is offset by the concomitant larger diffusion range. The ineffectual contribution of the outer-layered PAM antenna is consistent with the idea that the effect of PAM antennae is distance dependent, further confirming the importance for PAM sequences to form a local microenvironment around the target to enhance cleavage.

We next investigated how the density of PAM in the microenvironment affects target cleavage. To this end, we constructed PAM-richer origami harboring more PAMs on every antenna strand (Fig. 5A, right). Topographic profiles of AFM images of PAM-richer antenna revealed a central area of identical width to that of the two-layered PAM-rich origami, but with a considerably increased height (Fig. 5E). Single-molecule cleavage kinetics of PAM-richer origami led to increased cleavage efficiency when compared to that observed with two-layered PAM origami (Fig. 5F). Simulations were conducted to model the effect of PAM density within the same PAM spatial range (18 nm by 18 nm). We found that the appearance probability of unbounded Cas9 was further increased in areas near the center of PAM antenna when the PAM density was increased (Fig. 5G), consistent with the observed enhanced target cleavage. Together, these results showed that higher density of PAM within the effective distance could further enhance target cleavage efficiency, because more PAMs increase the ability to recruit Cas9 molecules that could diffuse to the target site. The positive correlation between PAM density and target cleavage efficiency indicates that it is possible to regulate the microenvironment through arrangement of PAMs.

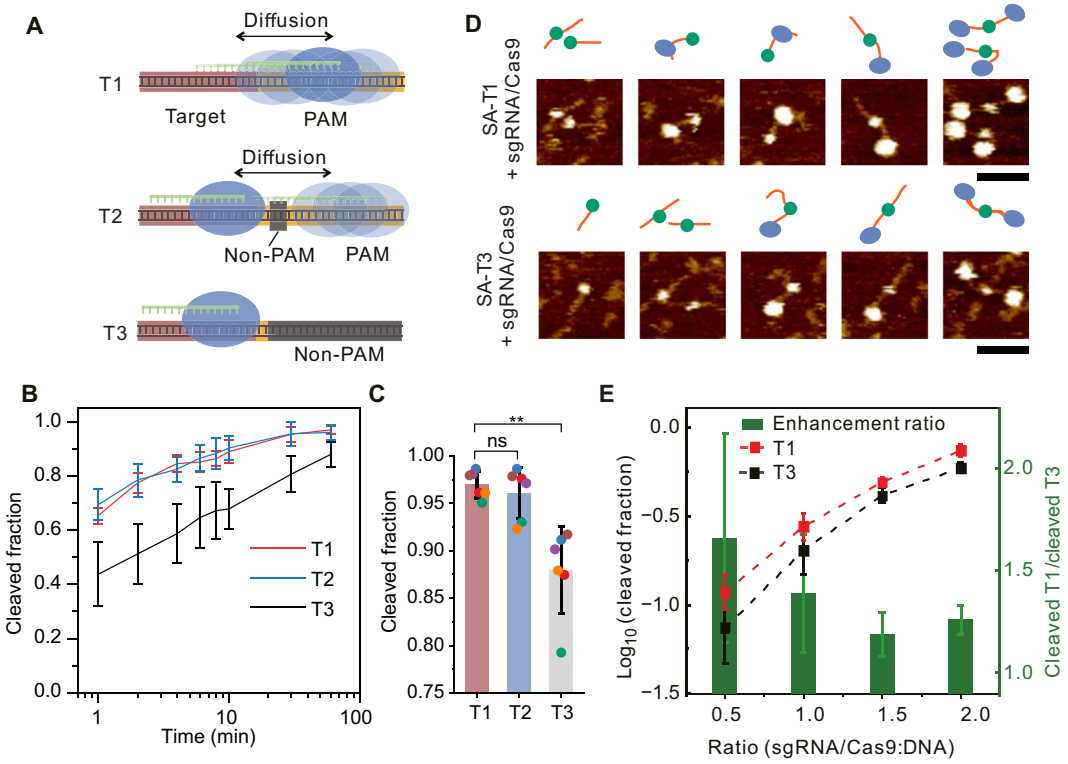

Fig. 6. Target cleavage efficiency enhancement with linear adjacent PAM antenna. (**A**) Schematics show sgRNA/Cas9 binding process on target flanking by linear PAM antenna containing eight tandem PAMs (T1), target separated with PAM antenna by 6-bp spacer (T2), and target flanking by non-PAM sequence (T3). (**B**) Averaged cleavage fraction of target from independently repeated experiments confirms cleavage efficiency enhancement with adjacent linear PAM antenna. Error bars represent SD for three independent experiments. (**C**) Final cleaved fraction of T1, T2, and T3 from six repeated experiments. Data from different experiments are indicated by different colors. The *P* values were calculated by paired two-sided *t* test ($n = 6$), where ns means $P > 0.05$ and $^{**}P < 0.01$. (**D**) AFM images of T1 and T3 at 2 nM incubated with 20 nM sgRNA/dCas9 showing that the binding position varies on T1, while dCas9 occupies a specific position on T3. (**E**) Cleavage fraction of T1 and T3 with 0×, 0.5×, 1×, and 2× sgRNA/Cas9 (red and black; left *y* axis) and cleavage enhancement ratio with PAM antenna (green; right *y* axis). Error bars represent SD for three independent experiments.

Programming PAM antenna for bulk CRISPR-Cas9 editing

Having substantiated the target cleavage enhancement of PAM microenvironments at the single-molecule level, we next tested whether the PAM microenvironment could be programmed for more efficient gene editing in bulk. We designed linear PAM antennae (in the PAMs are present in cis with the target) either adjacent to the target site (T1; Fig. 6A) or separated from the target site by a 6-bp non-PAM sequence (T2). For comparison, we synthesized a target with non-PAM adjacent sequence (T3). These targets were designed to mimic targets flanked by PAM-containing and non-PAM–containing sequences within the genome.

To explore whether a linear PAM microenvironment can enhance target cleavage in bulk, we performed cleavage assays using polyacrylamide gel electrophoresis by incubating T1, T2, and T3 with the same concentration of sgRNA/Cas9. Gel analysis showed that both T1 and T2 were thoroughly cleaved after incubating with sgRNA/Cas9 at a 1:2 ratio for 1 hour, while a retained uncleaved band was observed for T3 (fig. S14B). We further monitored the cleavage kinetics by interrupting the incubation of targets and sgRNA/Cas9 at different time points. Quantification of cleaved fraction from repeated experiments showed that targets next to PAM antennae T1 and T2 were cleaved faster than T3 (Fig. 6B and fig. S14A). Final cleavage efficiency from repeated experiments of T1 (97 ± 1%) was higher than that of T3 (88 ± 5%). We note that this improvement effect is statistically significant ($P < 0.01$; Fig. 6C).

To better understand the enhanced sgRNA/Cas9 functionality, we investigated the effects of linear (in cis) PAM antennae on target search process. We performed Markov chain simulations to study the distribution of Cas9. Heatmaps of Cas9 distribution showed enhanced intensity near the antennae, suggesting that a binding hotspot was formed by the linear PAM antennae (fig. S15). We next conducted binding observations using T1 and T3 to investigate whether the linear antennae adjacent to target could increase binding efficiency. To add polarity to the dsDNA target, we attached a streptavidin at one end (fig. S16). We found that a higher fraction of T1 was bound to dCas9 than of T3 (fig. S17), which is consistent with the hotspot effect of PAM antennae suggested by the simulations. Detailed investigation of the binding of Cas9 to these two types of targets showed that the binding positions varied on T1, while sgRNA/dCas9 occupied a fixed position on T3 (Fig. 6D). This observation indicates that linear PAM antennae can recruit Cas9 molecules that can be further translocated to the specific target site, contributing to increased cleavage efficiency. Comparing cleavage kinetics of T1 and T2, we found that both the cleavage speed and final cleaved fraction were indistinguishable for these two targets (Fig. 6B). The maintained enhancing effect of cleavage observed with T2 suggests that the short non-PAM spacer sequence between target site and the PAM antenna did not hinder the translocation of Cas9 (Fig. 6A, middle). The ability of Cas9 to cross non-PAM regions provides a wider target site selection range for more efficient gene editing.

To explore the effects of sgRNA/Cas9 concentration on target cleavage with and without PAM antennae, we incubated T1 and T3 with increasing levels of sgRNA/Cas9 and quantified the cleavage fractions from gel assays (Fig. 6E and fig. S14C). The higher cleavage efficiency observed for T1 than for T3 under each concentration condition suggests that gene editing could be achieved using less sgRNA/Cas9 through programming of PAM antennae. The ratio of cleaved fraction of T1 to T3 showed a higher cleavage enhancement ratio using PAM antennae at low sgRNA/Cas9 concentration (Fig. 6E), thereby potentially enabling more efficient gene editing when the delivery efficiency of CRISPR system is limited.

We further studied whether PAM antennae could influence off-target DNA cleavage. A mismatch 8-bp upstream PAM was introduced on T1 and T3 (M8-PAM and M8; fig. S18A). We found that the cleavage efficiency of M8-PAM was higher than that of M8 (fig. S18), suggesting that the presence of PAM antennae could also increase the cleavage of off-target sites, which may potentially reduce the specificity of gene editing. However, with the coexistence of target and off-target sites, the cleavage of target with M8-PAM did not differ from that with M8 (fig. S19A). In contrast, the cleavage of an off-target site (M8) was significantly decreased with T1 than with T3 (fig. S19B), suggesting that higher specificity could be achieved with PAM antennae at target site and avoiding PAM antennae at potentially off-target sites.

DISCUSSION

In this work, we designed PAM antennae in spatial proximity with a Cas9 target site on a DNA origami platform. We studied the effect of PAM antennae on target binding and cleaving. We find that PAM antennae anchored spatially close to the target enhance the local Cas9 distribution by recruiting more Cas9 molecules around the target, which, in turn, results in higher target cleavage efficiency. On the basis of the antenna effect on DNA origami, we designed a linear PAM antenna adjacent to target sequence and achieved enhancement of target cleavage in bulk.

Structured microenvironments have been shown to be critically important in many biochemical reactions both in vitro and in vivo. However, the effect of PAM microenvironments on CRISPR-Cas9 gene editing has hitherto largely been neglected. Extensive efforts have been focused on the sequence and structure optimization of Cas9, guide RNA, and the recognition site to achieve higher gene-editing efficiency. Progress has also been made through chemical modulation or DNA replacement of guide RNA. However, gene-editing efficiency needs to be further enhanced to improve in vivo applications of CRISPR. Here, we find that fine-tuning the PAM microenvironment affords a new route to improve the efficiency of gene editing. By programming PAM antennae, we achieved improvement in binding and cleavage efficiency, providing a new paradigm for the optimization of CRISPR-Cas9 targeting sites. Moreover, this approach can be combined with other strategies, including Cas9 optimization and guide RNA modification, to achieve more efficient genome editing in future work.

Our data also reveal that Cas9 bound to a PAM antenna can cross short non-PAM spacer sequences (perhaps by linear diffusion), allowing a much wider selection range of target sites that are not directly flanked by PAM antennae. As each chromosome in the human genome has an uneven distribution of PAMs, the nanoscale local PAM environment surrounding each targeting site could affect the cleavage efficiency differently. A detailed inspection of chromosome 1 showed that PAM intensity varies from 0 to 40 per 100 bp (fig. S20), the range of which is consistent with the number of PAMs in our experiments, suggesting that programming PAM antennae has potential for improving genome editing efficiency and specificity.

Taking advantage of DNA origami, DNA editing process was studied with different PAM antennae mimicking the three-dimensional microenvironment of chromatin. Three-dimensional characterization of genome structures showed that chromosomes are folded into highly packed topological-associated domains and long-range loops (*31*). A previous study reported that a 5 kbp locus could form a highly condensed structure less than 35 nm in diameter (*32*). The effects of PAM antennae found here suggest that PAM microenvironments surrounding the target in the context of chromatin should play an important role for in vivo gene editing. Using the antenna effects of PAM-rich microenvironment may facilitate efficient gene editing with a lower concentration of sgRNA/Cas9, which may further reduce the burden of delivery and the impact on cell activities, and advance the utility of the CRISPR-Cas9 genome editing system for practical purposes.

MATERIALS AND METHODS

Preparation of sgRNA

An optimized version of sgRNA proposed by Huang *et al.* (*33*) was used with customized DNA matching region. To prepare sgRNA, we prepared a dsDNA template containing the T7 promoter by polymerase chain reaction (PCR) amplification of a pair of forward and reverse primers using KOD polymerase (Toyobo; table S1). The product was purified using an agarose gel DNA extraction kit (TaKaRa, 9762). The obtained template was used for further transcription using an in vitro transcription T7 kit (TaKaRa, 6140). The sgRNA was purified using TRIzol (Invitrogen, 15596018) according to the manufacturer's instructions. The purified sgRNA was stored at −80°C.

Preparation of DNA origami with designed target site and antennae

Staples purchased from Sangon Biotech (Shanghai) were dissolved in deionized water, and stored in 100 μM at −20°C. Extended staples (table S2) for target and antennae were premixed to 1 μM. Original staples were premixed to 500 nM, and edge staples were removed to avoid stacking force while annealing. The origami folding mixture (100 μl) was prepared by mixing M13mp18 (to 2 nM; New England Biolabs, N4040S), extended staples (to 10 nM), and original staples (to 10 nM) in 1× TAE-Mg^{2+} buffer (40 mM tris, 2 mM EDTA, and 12.5 mM $MgAc_2$). The mixture was annealed using PCR Thermal Cycler (Applied Biosystems) with the following procedure: 95°C for 3 min, 95° to 4°C at a rate of 0.1°C/10 s in 0.1°C steps, 4°C forever. The annealed mixture was incubated with 50× hybridization strands of the extended staples for 4 hours under room temperature. DNA origami was purified three times at 3000*g* for 10 min using 100K centrifugal filters (Millipore) in an Eppendorf centrifuge and stored at 4°C for further use.

Gel electrophoresis for cleavage kinetics

For cleavage kinetics analysis of T1, T2, and T3, mixtures containing 160 nM target and 320 nM sgRNA/Cas9 with 1× reaction buffer were prepared on ice and divided into 10-μl parts. Mixtures were incubated at 37°C, and one sample for each of the three targets was

taken at indicated time points: 0, 1, 2, 4, 6, 8, 10, 30, and 60 min. Samples taken out were put into a 70°C thermostat water bath immediately and incubated for 10 min to inactivate Cas9. After samples were all treated in 70°C, they were incubated with ribonuclease at 37°C for 30 min. Products were mixed with 2 μl of 6× loading buffer before loading to 10% polyacrylamide gel. The gel was run with a constant voltage of 120 V for 80 min. At the end of the run, the gel was stained with GelRed and imaged using G:Box Chemi-XL (Syngene). Cleavage efficiency analysis at each time point was performed using the Gels tool in the ImageJ software.

AFM measurements

For origami imaging, 3-μl samples (2 nM) were pipetted onto freshly prepared mica surface. After incubation for 3 min, the surface was washed three times with 1× TAE. AFM experiments were performed using a MultiMode Nanoscope VIII system (Bruker). AFM images were obtained using ScanAsyst-Fluid+ tips (Bruker) in PeakForce fluid mode. Height images were flattened with the NanoScope Analysis software, and profile data were obtained using ImageJ. Center height analysis to characterize dCas9 binding was performed using MATLAB (MathWorks). Detailed sample preparation protocol and data analysis can be found in Supplementary Methods.

TIRFM experiments

TIRFM imaging was performed using a Nikon N-STORM microscope endowed with an electron-multiplying charge-coupled device camera (Andor iXon Ultra 897) and a solid-state 561-nm excitation laser. Multi–band-pass filters (422 to 478 nm, 502 to 549 nm, 581 to 625 nm, and 674 to 686 nm) were used for collecting fluorescence emission. TIRFM imaging experiments were performed in imaging buffer (40 mM tris, 2.1 mM EDTA, 20 mM Hepes, 100 mM NaCl, 5 mM $MgCl_2$, and 12.5 mM $MgAc_2$) at 20°C. For target cleavage experiments, glass-bottom dishes (D-29-10-1-N; Cellvis) were treated using plasma cleaner to make it hydrophilic. DNA origami (10 μl, 0.2 nM) was placed on the glass surface and incubated for 5 min to attach on the surface. The excitation intensity was adjusted to guarantee that Cy3 labels could survive more than 100 frames. To monitor the cleavage kinetics, we set an automated acquisition procedure for 15 or 20 min with 20-s intervals. Survival time distributions and accumulated cleaved fractions were calculated by custom-written MATLAB (MathWorks) programs. Polyethylene glycol (PEG)–passivated coverslips (*34*) were used for sgRNA/dCas9 tracking experiments (see Supplementary Methods for biotin-PEG coverslip preparation). Movies were obtained to record sgRNA/dCas9 binding events on origami B and P. Binding events and single-particle tracking were performed using custom-written MATLAB programs (see Supplementary Methods for details).

SUPPLEMENTARY MATERIALS

Supplementary material for this article is available at http://advances.sciencemag.org/cgi/content/full/6/19/eaay9948/DC1

View/request a protocol for this paper from *Bio-protocol*.

REFERENCES AND NOTES

1. P. Mali, L. H. Yang, K. M. Esvelt, J. Aach, M. Guell, J. E. DiCarlo, J. E. Norville, G. M. Church, RNA-guided human genome engineering via Cas9. *Science* **339**, 823–826 (2013).
2. C. E. Nelson, C. H. Hakim, D. G. Ousterout, P. I. Thakore, E. A. Moreb, R. M. C. Rivera, S. Madhavan, X. F. Pan, F. A. Ran, W. X. Yan, A. Asokan, F. Zhang, D. S. Duan, C. A. Gersbach, In vivo genome editing improves muscle function in a mouse model of Duchenne muscular dystrophy. *Science* **351**, 403–407 (2016).
3. J. S. Gootenberg, O. O. Abudayyeh, M. J. Kellner, J. Joung, J. J. Collins, F. Zhang, Multiplexed and portable nucleic acid detection platform with Cas13, Cas12a, and Csm6. *Science* **360**, 439–444 (2018).
4. F. G. Jiang, J. A. Doudna, CRISPR-Cas9 structures and mechanisms. *Annu. Rev. Biophys.* **46**, 505–529 (2017).
5. W. Y. Jiang, D. Bikard, D. Cox, F. Zhang, L. A. Marraffini, RNA-guided editing of bacterial genomes using CRISPR-Cas systems. *Nat. Biotechnol.* **31**, 233–239 (2013).
6. J. W. Woo, J. Kim, S. I. Kwon, C. Corvalan, S. W. Cho, H. Kim, S. G. Kim, S. T. Kim, S. Choe, J. S. Kim, DNA-free genome editing in plants with preassembled CRISPR-Cas9 ribonucleoproteins. *Nat. Biotechnol.* **33**, 1162–1164 (2015).
7. C. Z. Long, J. R. McAnally, J. M. Shelton, A. A. Mireault, R. Bassel-Duby, E. N. Olson, Prevention of muscular dystrophy in mice by CRISPR/Cas9-mediated editing of germline DNA. *Science* **345**, 1184–1188 (2014).
8. H. Ma, N. Marti-Gutierrez, S. W. Park, J. Wu, Y. Lee, K. Suzuki, A. Koski, D. M. Ji, T. Hayama, R. Ahmed, H. Darby, C. Van Dyken, Y. Li, E. Kang, A. R. Park, D. Kim, S. T. Kim, J. H. Gong, Y. Gu, X. Xu, D. Battaglia, S. A. Krieg, D. M. Lee, D. H. Wu, D. P. Wolf, S. B. Heitner, J. C. I. Belmonte, P. A. Mato, J. S. Kim, S. Kaul, S. Mitalipov, Correction of a pathogenic gene mutation in human embryos. *Nature* **548**, 413–419 (2017).
9. H. F. Wang, M. La Russa, L. S. Qi, CRISPR/Cas9 in genome editing and beyond. *Annu. Rev. Biochem.* **85**, 227–264 (2016).
10. A. T. Raper, A. A. Stephenson, Z. C. Suo, Sharpening the scissors: Mechanistic details of CRISPR/Cas9 improve functional understanding and inspire future research. *J. Am. Chem. Soc.* **140**, 11142–11152 (2018).
11. H. Xu, T. F. Xiao, C. H. Chen, W. Li, C. A. Meyer, Q. Wu, D. Wu, L. Cong, F. Zhang, J. S. Liu, M. Brown, X. S. Liu, Sequence determinants of improved CRISPR sgRNA design. *Genome Res.* **25**, 1147–1157 (2015).
12. Y. Dang, G. X. Jia, J. Choi, H. M. Ma, E. Anaya, C. T. Ye, P. Shankar, H. Q. Wu, Optimizing sgRNA structure to improve CRISPR-Cas9 knockout efficiency. *Genome Biol.* **16**, 280 (2015).
13. K. Nishida, T. Arazoe, N. Yachie, S. Banno, M. Kakimoto, M. Tabata, M. Mochizuki, A. Miyabe, M. Araki, K. Y. Hara, Z. Shimatani, A. Kondo, Targeted nucleotide editing using hybrid prokaryotic and vertebrate adaptive immune systems. *Science* **353**, aaf8729 (2016).
14. J. H. Hu, S. M. Miller, M. H. Geurts, W. X. Tang, L. W. Chen, N. Sun, C. M. Zeina, X. Gao, H. A. Rees, Z. Lin, D. R. Liu, Evolved Cas9 variants with broad PAM compatibility and high DNA specificity. *Nature* **556**, 57–63 (2018).
15. H. Yin, C. Q. Song, S. Suresh, Q. Q. Wu, S. Walsh, L. H. Rhym, E. Mintzer, M. F. Bolukbasi, L. J. Zhu, K. Kauffman, H. W. Mou, A. Oberholzer, J. M. Ding, S. Y. Kwan, R. L. Bogorad, T. Zatsepin, V. Koteliansky, S. A. Wolfe, W. Xue, R. Langer, D. G. Anderson, Structure-guided chemical modification of guide RNA enables potent non-viral in vivo genome editing. *Nat. Biotechnol.* **35**, 1179–1187 (2017).
16. M. Labuhn, F. F. Adams, M. Ng, S. Knoess, A. Schambach, E. M. Charpentier, A. Schwarzer, J. L. Mateo, J. H. Klusmann, D. Heckl, Refined sgRNA efficacy prediction improves large- and small-scale CRISPR-Cas9 applications. *Nucleic Acids Res.* **46**, 1375–1385 (2018).
17. B. P. Kleinstiver, V. Pattanayak, M. S. Prew, S. Q. Tsai, N. T. Nguyen, Z. L. Zheng, J. K. Joung, High-fidelity CRISPR-Cas9 nucleases with no detectable genome-wide off-target effects. *Nature* **529**, 490–495 (2016).
18. M. D. Szczelkun, M. S. Tikhomirova, T. Sinkunas, G. Gasiunas, T. Karvelis, P. Pschera, V. Siksnys, R. Seidel, Direct observation of R-loop formation by single RNA-guided Cas9 and Cascade effector complexes. *Proc. Natl. Acad. Sci. U.S.A.* **111**, 9798–9803 (2014).
19. S. H. Sternberg, B. LaFrance, M. Kaplan, J. A. Doucina, Conformational control of DNA target cleavage by CRISPR-Cas9. *Nature* **527**, 110–113 (2015).
20. C. Anders, O. Niewoehner, A. Duerst, M. Jinek, Structural basis of PAM-dependent target DNA recognition by the Cas9 endonuclease. *Nature* **513**, 569–573 (2014).
21. G. Palermo, C. G. Ricci, A. Fernando, R. Basak, M. Jinek, I. Rivalta, V. S. Batista, J. A. McCammon, Protospacer adjacent motif-induced allostery activates CRISPR-Cas9. *J. Am. Chem. Soc.* **139**, 16028–16031 (2017).
22. P. W. K. Rothemund, Folding DNA to create nanoscale shapes and patterns. *Nature* **440**, 297–302 (2006).
23. W. D. Xu, P. Yin, M. J. Dai, Super-resolution geometric barcoding for multiplexed miRNA PRofiling. *Angew. Chem. Int. Ed.* **57**, 14075–14079 (2018).
24. J. L. Fu, M. H. Liu, Y. Liu, N. W. Woodbury, H. Yan, Interenzyme substrate diffusion for an enzyme cascade organized on spatially addressable DNA nanostructures. *J. Am. Chem. Soc.* **134**, 5516–5519 (2012).
25. J. Chao, J. Wang, F. Wang, X. Ouyang, E. Kopperger, H. Liu, Q. Li, J. Shi, L. Wang, J. Hu, L. Wang, W. Huang, F. C. Simmel, C. Fan, Solving mazes with single-molecule DNA navigators. *Nat. Mater.* **18**, 273–279 (2019).
26. M. H. Räz, K. Hidaka, S. J. Sturla, H. Sugiyama, M. Endo, Torsional constraints of DNA substrates impact Cas9 cleavage. *J. Am. Chem. Soc.* **138**, 13842–13845 (2016).
27. N. C. Seeman, H. F. Sleiman, DNA nanotechnology. *Nat. Rev. Mater.* **3**, 17068 (2018).

28. N. G. Walter, C. Bustamante, Introduction to single molecule imaging and mechanics: Seeing and touching molecules one at a time. *Chem. Rev.* **114**, 3069–3071 (2014).
29. L. A. Gilbert, M. A. Horlbeck, B. Adamson, J. E. Villalta, Y. Chen, E. H. Whitehead, C. Guimaraes, B. Panning, H. L. Ploegh, M. C. Bassik, L. S. Qi, M. Kampmann, J. S. Weissman, Genome-scale CRISPR-mediated control of gene repression and activation. *Cell* **159**, 647–661 (2014).
30. S. H. Sternberg, S. Redding, M. Jinek, E. C. Greene, J. A. Doudna, DNA interrogation by the CRISPR RNA-guided endonuclease Cas9. *Nature* **507**, 62–67 (2014).
31. E. P. Nora, J. Dekker, E. Heard, Segmental folding of chromosomes: A basis for structural and regulatory chromosomal neighborhoods? *Bioessays* **35**, 818–828 (2013).
32. B. J. Beliveau, A. N. Boettiger, M. S. Avendaño, R. Jungmann, R. B. McCole, E. F. Joyce, C. Kim-Kiselak, F. Bantignies, C. Y. Fonseka, J. Erceg, M. A. Hannan, H. G. Hoang, D. Colognori, J. T. Lee, W. M. Shih, P. Yin, X. W. Zhuang, C. T. Wu, Single-molecule super-resolution imaging of chromosomes and in situ haplotype visualization using Oligopaint FISH probes. *Nat. Commun.* **6**, 7147 (2015).
33. B. H. Chen, L. A. Gilbert, B. A. Cimini, J. Schnitzbauer, W. Zhang, G. W. Li, J. Park, E. H. Blackburn, J. S. Weissman, L. S. Qi, B. Huang, Dynamic imaging of genomic loci in living human cells by an optimized CRISPR/Cas system. *Cell* **155**, 1479–1491 (2013).
34. A. Jain, R. J. Liu, Y. K. Xiang, T. Ha, Single-molecule pull-down for studying protein interactions. *Nat. Protoc.* **7**, 445–452 (2012).

Acknowledgments
Funding: This work was financially supported by the Ministry of Science and Technology of China (2016YFA0201200), the NSFC (grant nos. 21834007, 21722502, 21505045, and 21705048), the Shanghai Municipal Education Commission–Gaofeng Clinical Medicine Grant Support (20171913), and the Nanomachines program (KC1203) funded by the Office of Basic Energy Sciences of the U.S. Department of Energy (DOE) contract no. DE-AC02-05CH11231 (to C.B.). **Author contributions:** C.F. and C.B. directed the research. F.W., Y.H., and Q.L. performed the experiments. F.W., Y.H., Q.L., J.L., H.Z., X.Z., and L.W. analyzed the data. C.F., F.W., and C.B. conceived the experiment and wrote the manuscript. All authors read the manuscript and provided comments. **Competing interests:** The authors declare that they have no competing interests. **Data and materials availability:** All data needed to evaluate the conclusions in the paper are present in the paper and/or the Supplementary Materials. Additional data related to this paper may be requested from the authors.

Submitted 4 August 2019
Accepted 19 February 2020
Published 8 May 2020
10.1126/sciadv.aay9948

Citation: F. Wang, Y. Hao, Q. Li, J. Li, H. Zhang, X. Zhang, L. Wang, C. Bustamante, C. Fan, Programming PAM antennae for efficient CRISPR-Cas9 DNA editing. *Sci. Adv.* **6**, eaay9948 (2020).

Science Advances

Programming PAM antennae for efficient CRISPR-Cas9 DNA editing

Fei Wang, Yaya Hao, Qian Li, Jiang Li, Honglu Zhang, Xueli Zhang, Lihua Wang, Carlos Bustamante and Chunhai Fan

Sci Adv **6** (19), eaay9948.
DOI: 10.1126/sciadv.aay9948